

Chapter 5

AN HRE-BINDING POLYAMIDE IMPAIRS ADAPTATION OF TUMORS TO HYPOXIA

The text of this chapter was taken in part from a manuscript co-authored with Jevgenij A. Raskatov and Peter B. Dervan.

Abstract

Hypoxic gene expression contributes to the pathogenesis of many diseases, including organ fibrosis, age-related macular degeneration, and cancer. HIF-1, a transcription factor central to the hypoxic gene expression, mediates multiple processes including neovascularization, cancer metastasis, and cell survival. Py-Im polyamide 1 has been shown to inhibit HIF-1-mediated gene expression in cell culture but its activity *in vivo* was unknown. This study reports activity of polyamide 1 in subcutaneous tumors capable of mounting a hypoxic response and showing neovascularization. We show that 1 distributes into subcutaneous tumor xenografts and normal tissues, reduces the expression of several HIF-1-dependent proangiogenic and prometastatic factors, inhibits the formation of new tumor blood vessels, and suppresses tumor growth. Tumors treated with 1 show no increase in HIF-1a and have reduced ability to adapt to the hypoxic conditions, as evidenced by increased apoptosis in HIF-1a positive regions and the increased proximity of necrotic regions to vasculature. Overall, these results show that a molecule designed to block the transcriptional activity of HIF-1 has potent anti-tumor activity *in vivo*, consistent with partial inhibition of the tumor hypoxic response.

Introduction

Oxygen sensing is involved in a range of natural physiological processes such as embryonal development, wound healing, and immune response (1). However, its dysregulation can contribute to pathogenesis of multiple diseases including fibrosis, erythrocythemia, heart disease, and cancer – a group of diseases leading to nearly 600,000 deaths every year in the United States alone (2). While new cancer treatments are being developed (3, 4), many of the cancer therapies are hampered by presence of low levels of oxygen in tumors (5, 6), known as tumor hypoxia, regulated mainly by Hypoxia Inducible Factors (HIFs) (7). Among them - HIF-1 (8) – is a transcription factor that is often associated with poorer patient survival (5). HIF-1 orchestrates numerous aspects of cancer progression: tumor angiogenesis, cell survival in hypoxia, and metastasis (5, 9). Most inhibitors affect HIF-1 signaling indirectly, by targeting other proteins, including Topoisomerase I, mammalian target of rapamycin (mTOR), or microtubules (10). Established therapeutic strategies focus on modulating HIF-1 signaling by altering the HIF-1 protein levels (3, 10), its dimerization and protein interactions (11-14), or its DNA binding and transcriptional activity (15-18).

One method to inhibit transcriptional activity of HIF-1 is to displace it from its DNA-binding site, HIF-1 responsive elements (HREs), for example by echinomycin (15), or a molecule shown in this report (compound **1**, Fig. 5.1A) (16, 17). Compound **1** is a member of a class of DNA-binding small molecules, Py-Im polyamides, which can be programmed to recognize a broad repertoire of sequences with affinities and specificities comparable to those of transcription factors (19, 20). We reported that polyamides can modulate gene expression driven by many transcription factors in tissue culture (16, 17, 21-24). Our recent

mechanistic investigations expanded beyond the transcription factor:DNA interface, showing that Py-Im polyamides can induce degradation of the large subunit of RNA polymerase II, activation of the P53 stress response without concurrent DNA damage (25), and induction of DNA replication stress (26).

Experiments focused on HIF-1-DNA binding inhibition demonstrated the ability of **1** to displace the HIF-1 complex from DNA *in vitro* (16) , and by reducing HIF-1a occupancy at selected HREs in a common tissue culture model of hypoxic response - U251 cells as represented in Fig. 5.1B (17). When U251 cells were treated with Deferoxamine, a HIF-1 activator, **1** was capable of inhibiting 23% of the induced genes, establishing polyamide **1** as a partial inhibitor of HIF-1 transcriptional activity (17). The overall gene expression changes were distinct from other inhibitors, such as Echinomycin (15) or siRNA targeted to HIF-1a, but included many important proangiogenic factors, such as *VEGF*, *FLT1*, or *Endothelin-1*.

Our previous *in vivo* investigations demonstrated the bioavailability of various Py-Im polyamides upon intravenous (27), intraperitoneal, and subcutaneous administration (28). Subsequent *in vivo* xenograft studies established that polyamides could accumulate in subcutaneously grafted tumors (24, 29, 30), modulate tumor gene expression (24, 29), and inhibit growth of prostate cancer xenografts (25, 31).

We sought to evaluate the mechanism of action of **1** *in vivo* and its therapeutic potential in treatment of cancer and other HIF-1-related diseases. We hypothesized that **1** could act as a partial inhibitor of HIF-1a-driven gene expression *in vivo*, thus inhibiting tumor growth and angiogenesis. We chose a subcutaneous tumor model, due to its hypoxic nature (5) and reliability of measurements in angiogenesis, tumor growth, and gene expression. The cell

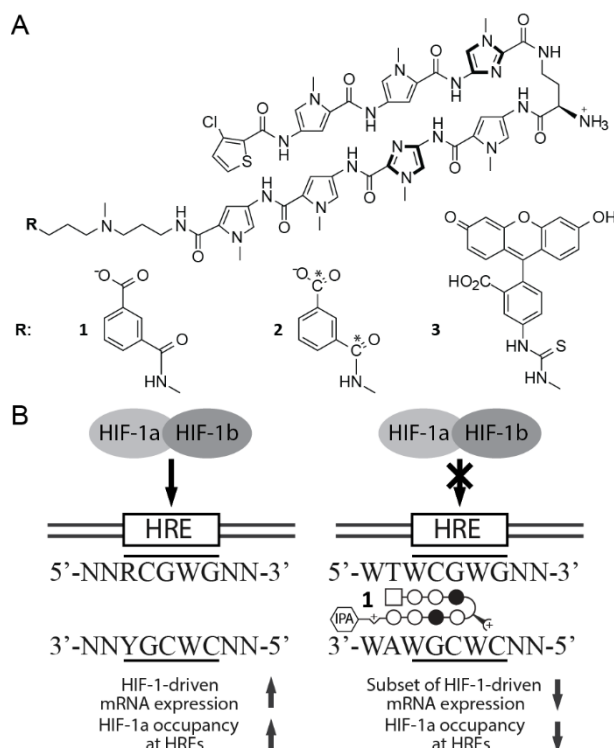


Figure 5.1 Chemical structure and biological activity of Py-Im polyamides binding HRE sequence. A) Chemical structures and ball-and-stick representation of the Py-Im polyamides **1-3**. N-methylpyrrole, N-methylimidazole and chlorothiophene are represented as open circles, filled circles and squares, respectively. B) Our previous studies (18) indicated that compound **1** can bind to HRE-containing sequence with nanomolar affinity and displace HIF-1 complex from in VEGF and CA9 promoters in U251 cells.

lines chosen for engraftment have been evaluated extensively in xenograft models of cancer (32-34), and hypoxic gene expression in one of them (U251) can be regulated by **1** (17) and Echinomycin (15), making it a good choice for evaluating *in vivo* mechanism of action of **1**. The second cell line, GBM39 (35), was derived from the same site as U251 cells (brain), but was maintained as subcutaneous xenografts and expanded in serum-free conditions as spheroids. The serum-free treatment maintains genetic and histologic variability of human tumors (36) and was thus our choice to ascertain the generality of the mechanism of action of polyamide **1**. The distinct profile of gene expression modulation,

favorable pharmacokinetics, and ability to modulate some aspects of hypoxic response

by **1**, could establish it as an interesting candidate for treatment of HIF-1 related diseases.

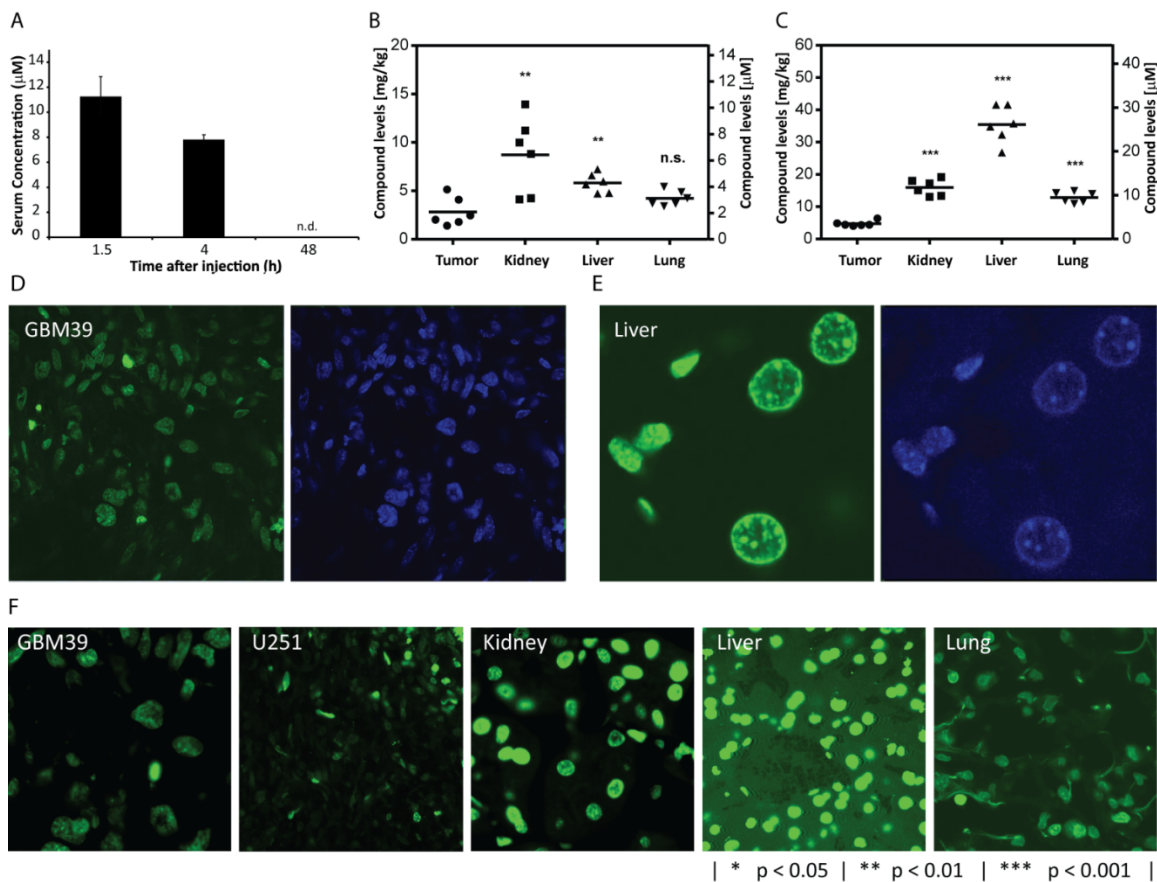


Figure 5.2. Pharmacokinetics, tissue distribution of and nuclear uptake of compounds 1-3 in-vivo. A) Serum concentration of **1** after subcutaneous injection. The C57BL6 mice were injected with **1** subcutaneously into interscapular area, after which we drew blood via retroorbital collection (n=4 per time point). B) GBM39 tumor bearing mice were injected I.P. with a 6.8mg/kg of C-14 radiolabeled polyamide **2**. The tissues were harvested 24-hours post-injection, weighed, dissolved, and quantified by scintillation. The absolute scintillation counts are normalized to organs' weight. C) GBM39 tumor bearing mice were injected I.P. with 6.8mg/kg of **2** (*Schedule A, intraperitoneal*) labeled with a radioactive C-14, harvested, and quantified 24 hours after the last injection. D) Compound **3** was injected S.C. into interscapular area at 5 $\mu\text{M}/\text{kg}$ (*Schedule A*) and tissues were harvested 24 hours after the last injection. The compound **3** showed nuclear uptake in GBM39 xenograft sections. E) Compound **3** shows nuclear staining consistent with distribution of chromatin in the nucleus. F) Uptake of **3** into the tissues showing nuclear staining. The tissues were harvested 24 hours after last injection fixed with 10% NBF, co-stained with DAPI, and imaged. The left panel shows FITC channel, showing nuclear uptake of **3**, and the right panel shows a DAPI co-stain showing chromatin. Error bars denote 95% CI.

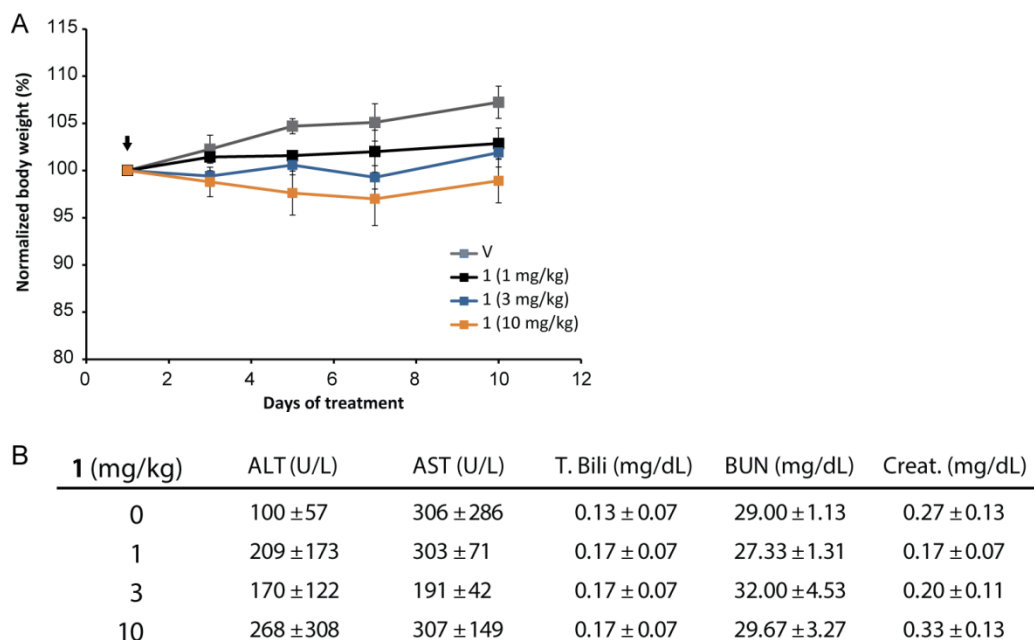


Figure 5.3 Py-Im polyamide **1** single-dose escalation study of toxicity. A) The C57BL6 mice were injected with **1** subcutaneously and their weights were measured on days 3, 5, 7 and 10 (n=3 per condition). The maximum weight loss has been observed for **1** dosed at 10 mg/kg, reaching an average of 3% (+/- 1.4) below the original mice weight. The weight loss for the other groups was below 1% throughout the study. Arrow denotes an injection. B) A single injection of **1** was administered at doses 1-10 mg/kg in C57BL6 mice. After 10 days, blood was drawn retroorbitally, serum was cleared by centrifugation and samples submitted for analysis of serum toxicity markers. No significant changes in any of the tested markers were observed after injection of **1**. Error bars and uncertainty values denote 95% CI.

Results

Py-Im polyamide 1 shows favorable preliminary pharmacokinetics and tissue distribution at tolerable doses. In order to evaluate bioavailability of **1** *in vivo*, we injected it subcutaneously (s.c.) at 6.8 mg/kg into C57BL6 mice. Compound **1** reached a serum concentration of 11.3 ± 1.6 μM within 1.5 h and 7.8 ± 0.4 μM at 4 h post-injection (Fig. 5.2A). A single-injection toxicity test showed that **1** did not affect animal weight, or levels of serum toxicity markers (ALT, AST, TBIL, BUN, Creat) at concentrations up to 10 mg/kg (Fig. 5.3A, B), indicating that this compound could be used *in vivo* without

significant toxicity. Taken together, these results supported evaluation of anti-tumor effects of **1** *in vivo*. The radiolabeled analogue of **1**, Py-Im polyamide **2**, was injected intraperitoneally (IP) to quantitate whole-organ compound concentrations (Fig. 5.2B, C) into immunocompromised NSG mice bearing GBM39 tumors. After 24 h, concentrations of **2** were measured in GBM39 xenografts (2.0 μM), host's kidney (6.3 μM), liver (4.2 μM) and lung (3.1 μM ; Fig. 6.2B). Following 3 injections (*Schedule A*, 6.8mg/kg s.c., every other day x 3, harvest 72h post last injection), all tested tissues showed compound accumulation (Fig. 6.2C). Administration of **3** (FITC-conjugate of **1**), according to *Schedule A* in NSG mice, resulted in readily detectable nuclear staining in tumors (U251, Fig. 6.4A; GBM39, Fig. 6.2D) and tested tissues (Fig. 6.2E-F).

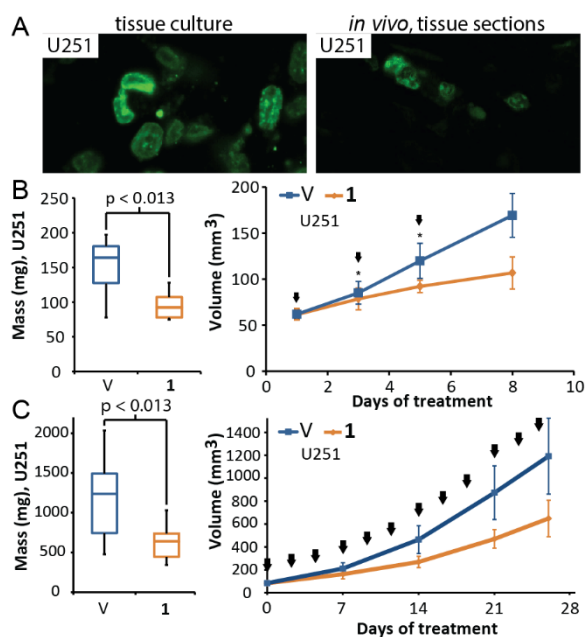


Figure 5.4 Polyamide 1 inhibits tumor growth. A) Uptake of **3** in U251 cells in tissue culture, and in s.c. xenograft sections. B) Final masses and growth curve of s.c. U251 xenografts derived from animals subjected to *Schedule A* (n=7,8, for vehicle and treated groups; for volumes, measurements at the 3rd and 5th day contain 5 data points.) C) Final masses and growth curve of U251 xenografts (*Schedule B*, n=10 per condition). Arrows denote injections. Error bars are 95% CI for growth curves and minimum-maximum values for mass graphs.

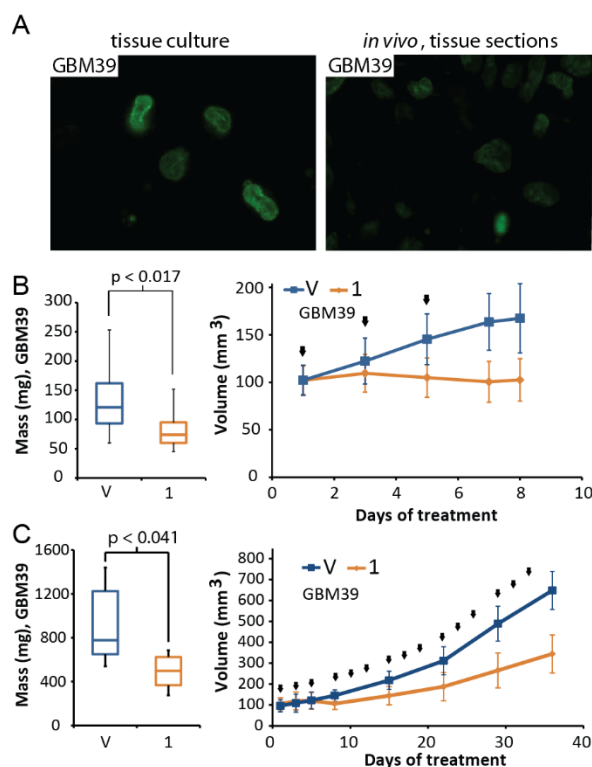


Figure 5.5 Py-Im polyamide 1 shows nuclear uptake and attenuates tumor growth in GBM39 xenografts. A) Uptake of **3** in GBM39 cells in tissue culture, and in xenograft sections. B) Final masses and growth curve of s.c. GBM39 xenografts derived from animals subjected to *Schedule A* (n=11, per condition). C) Final masses and growth curve of s.c. GBM39 xenografts (*Schedule B*, n=6 per condition). Arrows denote injections, error bars denote 95% CI for growth curves, and minimum-maximum for final mass plots.

Polyamide 1 suppresses tumor growth in subcutaneous xenografts. To test whether previously established partial inhibition of HIF-1-driven gene expression by **1** (**17**) would result in a decrease in tumor growth, we engrafted U251 and GBM39 cells s.c. into NOD/SCID- γ (NSG) mice. We established three dosing regimens for **1** – *Schedule A*, consisting of three s.c. injections every other day at maximum tolerated dose (6.8 mg/kg, 8 days) and *Schedules B and C*, with lower dose (4.5mg/kg, 3 inj./week) designed for prolonged treatment with low weight loss (<10%) over 4 weeks (U251 tumors) or 6 weeks (GBM39 tumors). In all cases, the tumors were harvested 72 h after last injection.

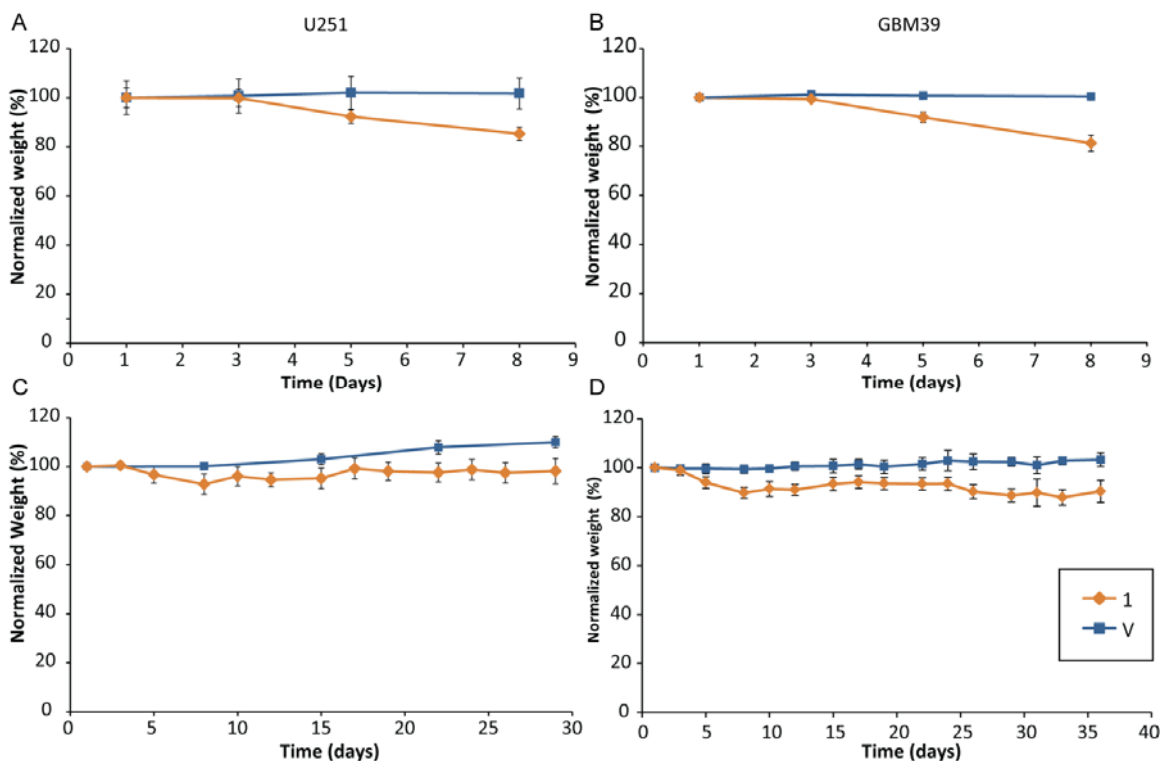


Figure 5.6. Mouse weight loss during treatment with Py-Im polyamide 1. A) Mice bearing U251 xenografts were injected with 6.8 mg/kg of **1** on the 1st, 3rd and 5th day of treatment (*Schedule A*). The weight was recorded and normalized to the initial weight for vehicle (n=7) and polyamide treated (n=8) mice. B) Analogous weight measurement of mice bearing GBM39 xenografts, treated with **1** according to schedule A (n=11, per condition). C) Weight measurements of mice with U251 tumors, treated with Py-Im polyamide **1** over 4 weeks (*Schedule B*) and of mice bearing GBM39 xenografts (D), treated with **1** according to *Schedule C*. Error bars denote 95% CI.

Mice bearing U251 tumors that were subjected to treatment with **1** (*Schedule A*) showed a median tumor burden reduction amounting to 1.8-fold ($p < 0.013$; n=7, 8 for vehicle and treated groups; Fig. 6.4B;) compared to vehicle. Similarly, prolonged treatment (*Schedule B*) resulted in 1.9-fold lower median U251 tumor mass ($p < 0.0125$; n=10 per condition; Fig. 6.4C). Consistent results were obtained with a primary glioma cell line (GBM39) xenograft.

Treatment according to *Schedule A* resulted in 1.8-fold lower median mass ($p < 0.016$; $n = 11$ per condition; Fig. 6.5A) and prolonged treatment (*Schedule C*) in 1.6-fold reduction ($p < 0.041$; $n = 6$ per condition; Fig. 6.5B). The treatments resulted in minor mouse weight loss; the effects were less severe ($< 5\%$ average w.l. throughout the experiment) for schedules *B* and *C* (Fig. 6.6).

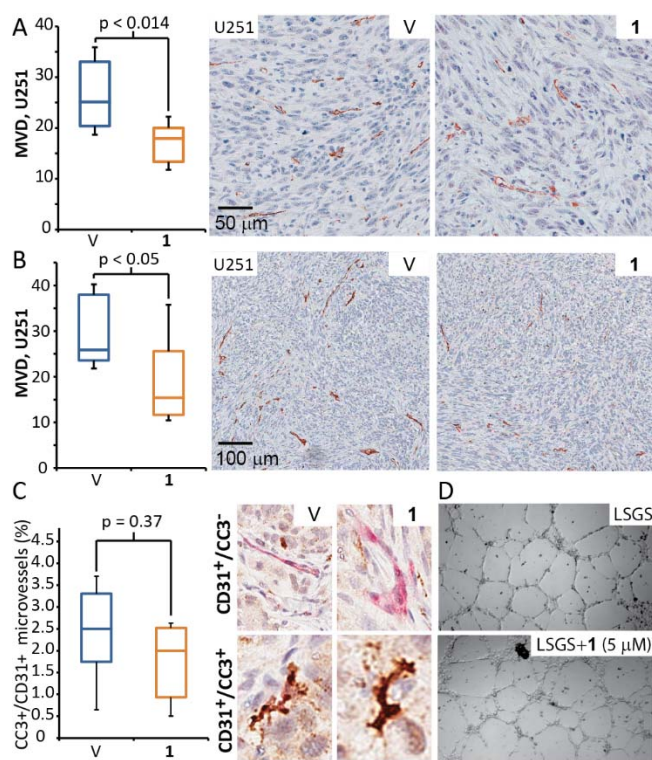


Figure 5.7 Polyamide 1 reduces microvessel density in tumors, without affecting blood vessel apoptosis or HUVEC tube formation on matrigel. A) Mice harboring xenografts were treated with 1 according to *Schedule A* and their MVD score was measured using anti-mouse CD31 immunostaining of tumor sections (For U251 $n = 7, 8$ for vehicle, and treated groups). B) Prolonged treatments, according to *Schedule B* in U251 xenografts led to comparable decrease in MVD. C) Apoptosis in blood vessels was determined by double-staining of Cleaved Caspase-3 (CC3) and mouse CD31 of GBM39 tumor sections treated according to *Schedule C*. Both vehicle and polyamide-1 treated samples exhibited low levels of blood vessel apoptosis and the differences between the groups were not significant ($p = 0.37$, $n = 5$ per condition). D) An *in vitro* angiogenesis assay - matrigel tube formation assay using HUVECs - shows treatment with 1 ($5 \mu\text{M}$) over

48h has no effect on endothelial tube formation. Error bars denote minimum and maximum.

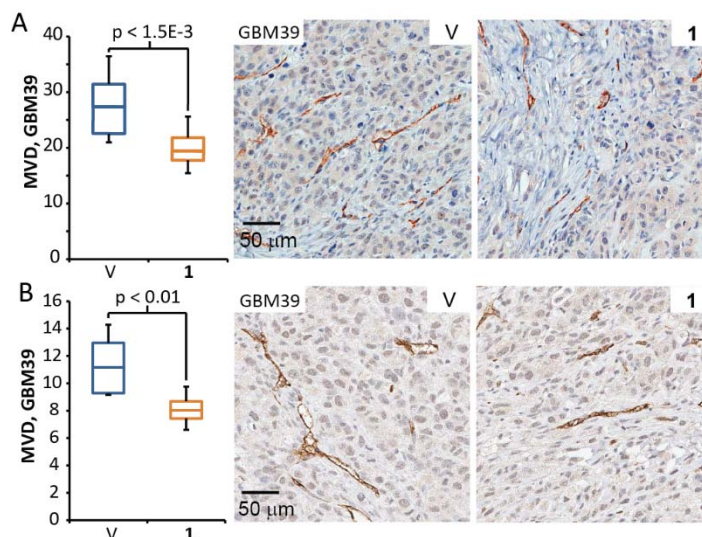


Figure 5.8 Polyamide 1 reduces microvessel density of GBM39.

A) GBM39 tumors treated with **1** according to *Schedule A* show 1.4-fold reduction of MVD at the endpoint ($p < 0.0015$; $n = 11$ per condition). Similarly, when treated according to *Schedule C*, the same level of reduction was observed ($p < 0.01$; $n = 6$ per condition). Error bars denote minimum and maximum.

Polyamide 1 reduces microvessels density in xenografts, without inducing endothelial apoptosis. Hypoxic signaling is a major driver for angiogenesis and its inhibition leads to a decrease in microvessel density (MVD) (1, 10). We measured MVD using anti-mouse CD31 immunostaining of tumor sections. We observed a significant reduction of MVD in all tested scenarios. For U251 tumors, with mice subjected to *Schedule A*, we observed a 1.4-fold median reduction of MVD ($p < 0.014$; $n = 7,8$ for vehicle and treated groups; Fig. 6.7A) and a 1.7-fold median decrease for *Schedule B* ($p < 0.05$, $n = 10$ per condition; Fig. 6.7B). For GBM39 tumors, both treatment schedules (A and C) led to a 1.4-fold reduction in MVD ($p < 0.01$; $n = 11$ and $n = 6$ for *Schedule A* and C; Fig. 6.8).

The decrease in MVD could be caused by direct effect of **1** on the endothelium, for example, rendering it either apoptotic, or unable to form blood vessels. We evaluated endothelial apoptosis by double-staining of mouse-specific CD31 and Cleaved Caspase-3 (CC3) in GBM39 tumors (Fig. 6.7C, *Schedule C*). We found no significant endothelial apoptosis in either of the treatment groups. To measure angiogenic functionality of endothelium we used *in vitro* matrigel tube formation assay with Human Umbilical Cord Endothelial Cells (HUVEC), revealing **1** (5 μ M, 48 h) had no effect on tube formation (n=3, Fig. 6.7D).

Antiangiogenic effects of 1 are associated with inhibition of several aspects of hypoxic response. Decrease in MVD, without endothelial apoptosis or dysfunction, suggests **1** could interfere with the hypoxic response in tumors and possibly its primary regulator – HIF-1 (8). To further test this hypothesis we evaluated other aspects affected by hypoxic response, such as tumor cell proliferation (6), apoptosis in HIF-1 positive, perinecrotic areas (6), nuclear HIF-1 α protein accumulation, and cell survival in areas distant from blood vessels (37, 38). To analyze this, we divided the tumor sections into three areas: necrotic, non-necrotic, and perinecrotic (Fig. 6.9A). The non-necrotic areas contain viable cells, while necrotic areas are decellularized. The perinecrotic area represents field of view (20x magnification) on the verge between necrosis and non-necrosis.

Antiangiogenic therapy increases hypoxia in tumors and often leads to decreased proliferation (37, 39). Upon treatment with **1** (*Schedule B*), we observed a 1.2-fold decrease ($p < 0.05$; Fig. 6.9B) in proliferation marker (Ki-67) in non-necrotic areas of the U251

tumors.

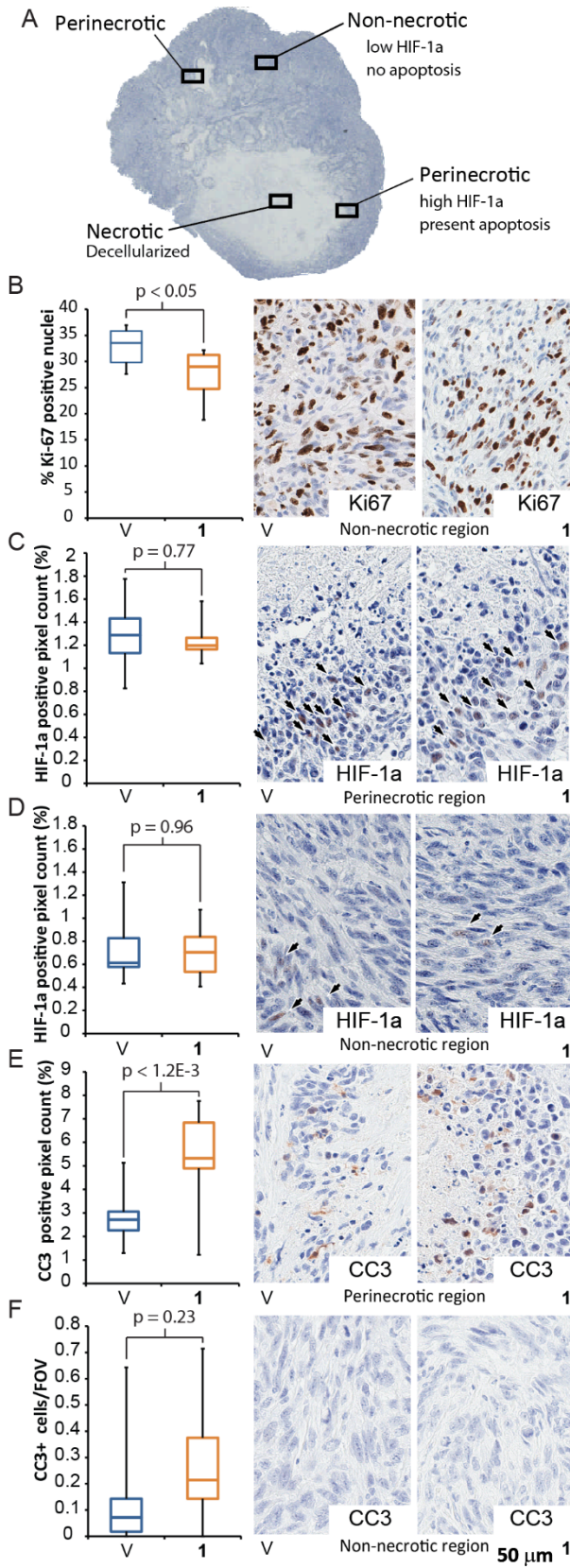


Figure 5.9 Treatment with 1 decreases tumor proliferation, induces apoptosis in HIF-1a positive areas and does not lead to HIF-1a accumulation. A) Regions used for local analysis in U251 tumors (*Schedule B* treatment). All analysis was done at 20x magnification; perinecrotic area contained 50% necrosis and 50% adjacent, non-necrotic area, as shown. B) Treatment with 1, induced a modest, but statistically significant decrease in proliferative index (Ki-67 staining). C) Non-necrotic tumor regions show no presence of apoptosis. However, cells in perinecrotic region show significant increase in CC3 staining upon treatment with 1 (D). Similarly, non-necrotic region exhibited low numbers of HIF-1a positive pixels (E) and perinecrotic area was more positive in HIF-1a (F). However, there were no differences in HIF-1a levels between the treatment groups. For each measurement $n=10$, per condition. Error bars denote minimum and maximum.

Another effect of induction of hypoxic response is accumulation of HIF-1a (1). However, treatment with **1** did not lead to an increase in levels of HIF-1a in either U251 (Fig. 6.9C, D) or GBM39 (Fig. 6.11A, B) tumors. Lack of HIF-1a accumulation is unlikely to be caused by its increased degradation, as **1** does not affect HIF-1a levels in tissue culture (Fig 11C). Overall, we observed a spatial distribution of HIF-1a in U251 tumor sections: perinecrotic areas showed higher HIF-1a levels compared to non-necrotic areas (1.8-fold average increase for **1**; $p < 0.001$, Fig 9C, D).

Induction of hypoxic signaling can lead to apoptosis resistance in cancer cells (37). However, treatment with **1** increased apoptosis significantly in perinecrotic, HIF-1a positive, areas (1.8-fold, $p < 0.0012$; Fig. 6.9E). The apoptosis was absent in non-necrotic regions of U251 tumors regardless of the treatment (Fig. 6.9F), suggesting that **1** is toxic specifically to hypoxic cells.

Hypoxic signaling mediates cell survival in areas distant from blood vessels, where oxygen pressures are the lowest. With increasing distance to blood vessels, tumor necrosis appears as a result of the death of cells with inadequate oxygen supply (1, 40). Therefore, to measure if **1** decreases ability of cells to adapt to low oxygen pressures, we measured MVD as a function of distance from the edge of necrotic areas. We found the expected lack of microvessels nearby necrotic edges. However, tumors derived from animals treated with **1** (U251, *Schedule B*) showed greater microvessel densities in areas close to the edge necrosis (3.3-fold at 150 μm and 2.3-fold for 200 μm distance, $p < 0.02$ and $p < 0.01$, $n = 10$ per condition; Fig. 6.10A, B), suggesting that treated tumor cells could require a higher level of nutrients and oxygen for survival. Similarly, the median distances between a random

point at the edge of necrosis and the nearest blood vessels were significantly shorter in case of group treated with **1** for U251 ($p < 0.001$, *Schedule B*, $n = 10$ per condition; Fig. 6.11D) and GBM39 tumors ($p < 0.01$, *Schedule C*, $n = 6$ per condition Fig. 6.11D).

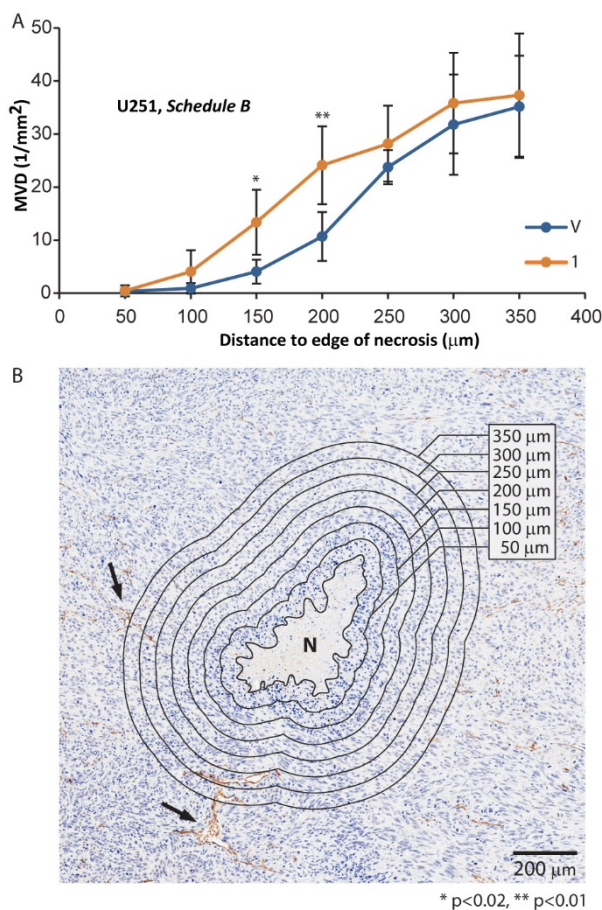


Figure 5.10. Treatment with **1** increased reliance of tumor cells on proximity to vasculature. Necrosis was delineated manually and zones were offset every 50 µm. Number of blood vessels per area was calculated for each zone and converted to MVD. A) Group treated with **1** shows higher MVD in perinecrotic areas - within 150 and 200 µm from the edge of necrosis. B) Example of necrosis along with delineation and zonal analysis of MVD. ($n = 10$ tumor per condition, 854 total microvessels measured for a group treated with **1** and 586 for a group treated with vehicle). Arrows denote two of the large microvessels, N denotes necrosis. Error bars denote 95% CI.

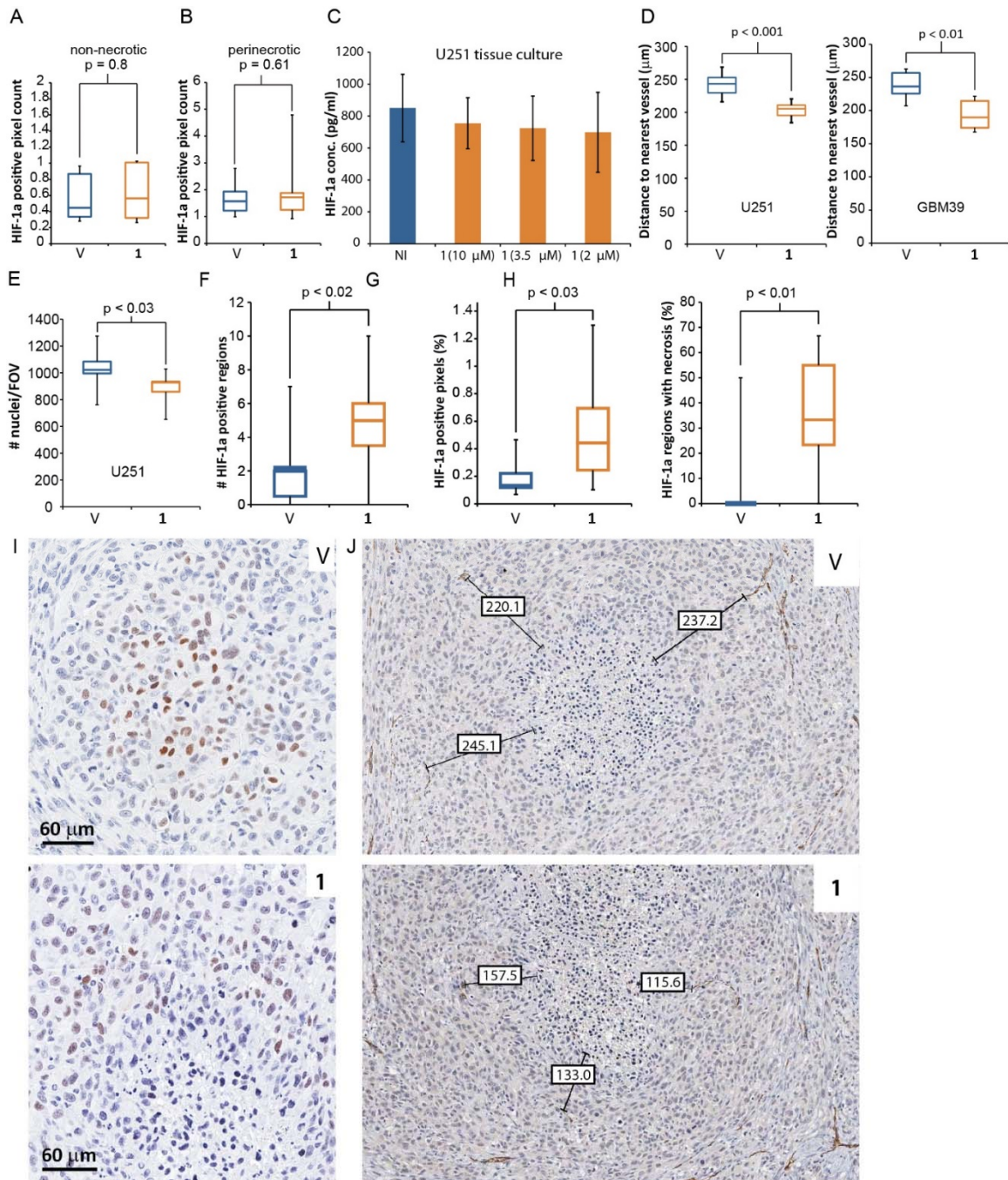


Figure 5.1 In vivo Effects of treatment with 1 are consistent between GBM39 and U251 xenografts. A) Non-necrotic region exhibited lower numbers of HIF-1a positive pixels (B) in comparison to perinecrotic region. However, we did not find increased levels of HIF-1a in treated samples, despite decreased microvessel density. C) The lack of HIF-1a induction in xenografts is unlikely to be caused by HIF-1a protein degradation as 1 did not affect HIF-1a levels in U251 cells in tissue culture. D) For both U251 and GBM39 xenografts, we found an association between presence of necrosis and distance from the nearest CD31+ microvessel closely matching distances obtained

for U251 xenografts. Interestingly, GBM39 tumors treated with **1** according to *Schedule A* showed increased presence of areas positive in HIF-1a (F-H), which often contained necrotic center (I). Further analysis shows that necrosis occurs in regions that do not contain blood vessels (J). Numbers in boxes denote distance between edge of necrotic regions and the nearest microvessel (μm). Error bars for all panels except C) denote minimum and maximum. Error bars in the panel C) denote 95% CI.

Lower MVD and lower cell survival at a distance from blood vessels should lead to an increase in necrotic area. However, the complex pattern of necrosis (micronecroses) in U251 tumors made it difficult to quantify it by a simple delineation. Instead, we decided to automatically count nuclei in the whole tumor section and found lower nuclear density in tumors treated with **1**, (10% fewer nuclei, $p < 0.03$, Fig. 6.11E). Further evidence of necrosis induction by **1** was present after short-term treatment with **1** in GBM39 tumors (*Schedule A*) where transient accumulation of HIF-1a (Fig. 6.11F-H) led to presence of necrosis (Fig. 6.11I), specifically localized to HIF-1a positive areas that were distant from microvessels (Fig. 6.11I, J).

Overall, compound **1** decreases proliferation and nuclear density, selectively induces apoptosis in perinecrotic, HIF-1a positive areas, and causes necrotic areas to appear closer to vasculature, but treatment does not result in long-term HIF-1a accumulation.

Py-Im polyamide 1 reduces expression of proangiogenic and prometastatic factors in tumors. A common adverse effect of antiangiogenic treatment is upregulation of proangiogenic and prometastatic gene expression, which renders the antiangiogenic therapies less effective and is often a result of hypoxic signaling (4). We decided to test if **1** affected mRNA expression of such factors *in vivo*. NSG mice bearing U251 tumors (n=6 per condition) were treated with **1** according to *Schedule D* (6.8 mg/kg, 2 inj., on days 1

and 3; tumors harvested on day 5). Out of 10 tested proangiogenic factors, four transcripts had lower relative expression after treatment with **1** (Fig. 6.12A), and one (*VEGF*) was upregulated (1.4-fold) in both mRNA (Fig. 6.12B) and serum protein levels (Fig. 6.6C). Downregulation of mRNA expression was also apparent in the panel of prometastatic genes. Overall, 5 out of 6 tested transcripts were downregulated in the group treated with **1** (Fig. 6.12D). Results for all tested genes can be found in Table 1.

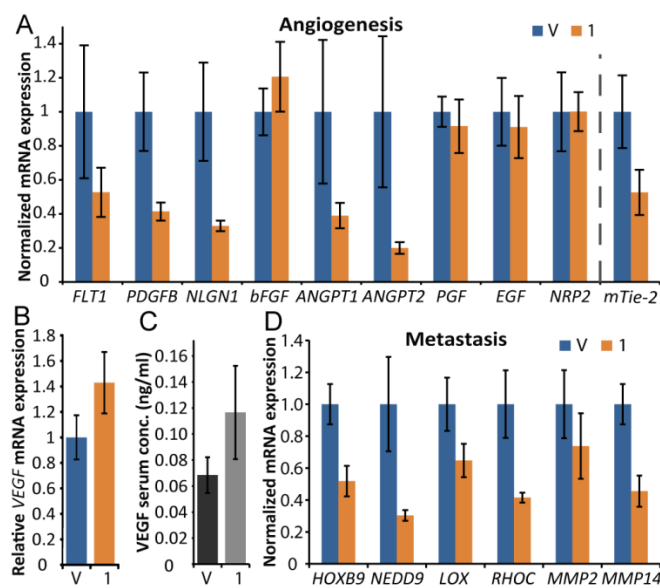


Figure 5.12. Treatment with **1 inhibits transcription of proangiogenic and prometastatic factors in tumors.** Mice harboring U251 tumors were treated according to *Schedule D* to capture gene expression profile underlying the changes in tumor mass and MVD (n=8 per condition). We registered a significant downregulation of several important proangiogenic factors (A), including Angiopoietins 1 and 2 (*ANGPT1*, *ANGPT2*), overall tumor levels of their receptor mouse-*Tie-2* (*mTie-2*), Neurologin 1 (*NLGN1*), as well as Plateled-Derived Growth Factor-B (*PDGFB*). Interestingly, both mRNA expression (B) and serum protein levels of a human-*VEGF* (C) were upregulated slightly in treated animals (n=8,6 for samples treated with vehicle and **1**). We selected a panel of prometastatic factors and found that **1** inhibits mRNA expression in all tested transcripts except *MMP2* (D). Error bars denote 95% CI.

Table 5.1 Percent changes in transcript expression of U251 tumors dosed with 1 according to *Schedule D* (n=8 per condition).

Gene	% change	CI95%	p-val
Significantly changed expression			
<i>ANGPT1</i>	-61.0	7.4	0.025
<i>ANGPT2</i>	-80.0	3.4	0.010
<i>HIF1a</i>	-33.8	15.3	0.005
<i>HOXB9</i>	-48.2	9.6	4.7E-05
<i>LOX</i>	-35.2	10.5	0.004
<i>mTie-2</i>	-49.4	8.4	0.003
<i>NEDD9</i>	-69.7	3.3	4.2E-04
<i>NLGN1</i>	-67.1	3.1	4.7E-04
<i>MMP14</i>	-54.4	9.7	0.000
<i>PDGFB</i>	-58.6	5.3	0.011
<i>RHOC</i>	-58.5	3.1	9.9E-05
<i>VEGF</i>	42.9	9.7	0.014
Unchanged expression			
<i>bFGF</i>	20.6	20.5	0.112
<i>BNIP3</i>	14.6	15.7	0.988
<i>CDH1</i>	not exp.	not exp.	n.d.
<i>CIDEA</i>	0.4	29.8	0.172
<i>EGF</i>	-8.9	18.2	0.528
<i>FLT1</i>	-47.3	14.5	0.053
<i>ITGA4</i>	-32.6	8.9	0.108
<i>MCJ</i>	-3.6	45.2	0.096
<i>MMP2</i>	-26.2	20.5	0.105
<i>NFKB</i>	-37.9	11.4	0.891
<i>NRP2</i>	0.1	11.5	0.996
<i>PGF</i>	-8.5	15.8	0.236

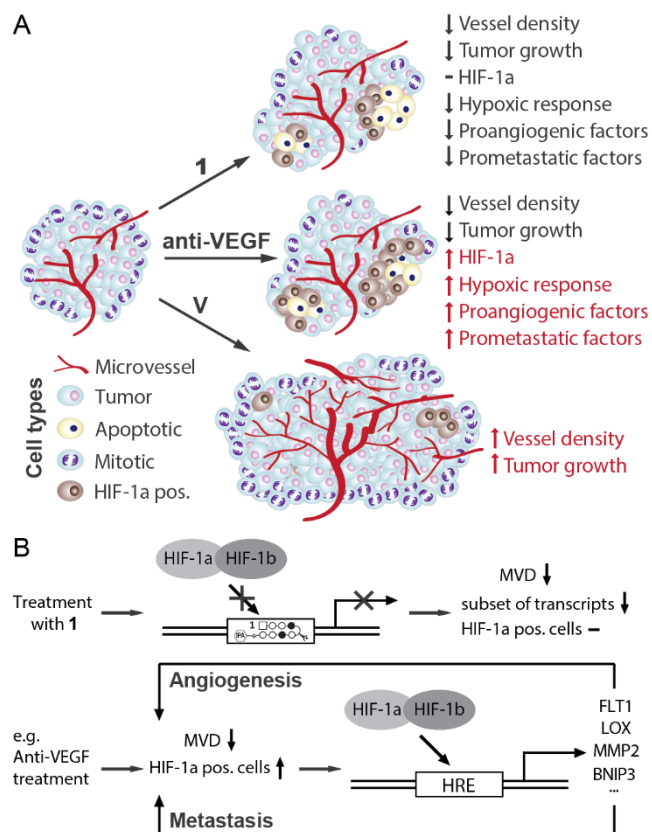


Figure 5.13. Treatment with 1 inhibits tumor growth and decreases density of vasculature in a distinct way compared to an anti-VEGF therapy. A) Compound 1 reduces microvessel density, hypoxia-related gene expression and cell proliferation, but does not increase HIF-1a levels. Presence of apoptosis in HIF-1a positive, but not HIF-1a negative, areas indicates increased sensitivity of cancer cells to hypoxia. This statement is supported by necrotic areas, being found closer to blood vessels after treatment with 1. B) Therapies targeting angiogenesis (e.g. Anti-VEGF) often lead to increased expression of prometastatic and proangiogenic factors because they do not inhibit hypoxic response. Targeting hypoxia-dependent transcription with 1 inhibits many of those factors, thus impairing adaptation of tumors to hypoxia.

Discussion

Regulation of hypoxic signaling is central to maintaining balance between health and disease. Its principal regulator, HIF-1, is essential for tumor initiation and progression, *e.g.*, vascularization, cell survival and metastasis (5, 41). Inhibition of HIF-1 activity has

suppressed tumor progression and reduced cancer resistance to available therapies (reviewed in (1, 5)). Our group has previously reported on the function of an HRE-binding Py-Im polyamide **1** as a partial inhibitor of HIF-1 dependent transcription in tissue culture (17). However, the *in vivo* activity and mechanism of **1** remained to be explored. We used Py-Im polyamide **1** (Fig. 6.1) to show that it inhibits tumor growth (Fig. 6.4), angiogenesis (Fig. 6.7), and several aspects of hypoxic response *in vivo* (Figs. 9 and 10). We also discovered inhibition of mRNA expression of proangiogenic and prometastatic factors that are often upregulated in hypoxic conditions (Fig. 6.12). We found that the effects of **1** are consistent with what would be expected in the case of a partial inhibition of hypoxic response (Fig. 6.13).

Polyamide tissue distribution and preliminary pharmacokinetics. Subcutaneous administration revealed that **1** distributes into serum within 1.5 h post-injection, with 31% drop in concentration 2.5 h later, indicating multi-hour long half-life. Even though **1** had favorable pharmacokinetics, its activity *in vivo* is likely dependent on the target tissue concentration. After three intraperitoneal injections (Schedule A), the radioactive analog **2** reached a concentration of 3.5 μM in GBM39 tumor and higher levels in other tissues. Concentrations attained for **1** in all tested tissues were thus higher than those used in our tissue culture studies (17).

Effects on tumor growth and vascularization. In the present study, inhibition of tumor growth and reduction in MVD was observed in two different cell types in response to treatment with **1**. The extent of these effects was comparable to ones exerted by Bevacizumab (42) in xenografts derived from U251 (39) and GBM39 cells (33).

Investigation of possible mechanisms of antiangiogenic action showed a lack of apoptosis in blood vessel lining, and no measurable influence on tube formation on matrigel. Lack of direct effects of **1** on endothelial cells suggests blood vessel recruitment might be impaired. One possible explanation is inhibition of expression of tumor-associated proangiogenic factors by **1**. However, systemic concentration of those proteins could also be affected.

Effects on apoptosis, proliferation and HIF-1a levels. Compound **1** induces apoptosis selectively, in HIF-1a-positive, perinecrotic areas. This suggests that **1** sensitizes cancer cells to hypoxia, which could occur by hypoxic response inhibition (5). Further support of this hypothesis is the lack of increase of HIF-1a positive cells in the tumors treated according to *Schedule B* and *C*. Since **1** did not affect HIF-1a levels in U251 cells in tissue culture, it is likely that numbers of HIF-1a positive cells were reduced as they went through apoptosis. Finally, increased reliance of cancer cells on proximity to vasculature once again suggests their hindered ability to adapt to low partial oxygen pressures, which is the main function of the hypoxic response. The transient induction of HIF-1a levels in briefly-treated GBM39 tumors could be due to two factors: concentration of **1** was insufficient to induce apoptosis of tumor cells in *Schedule A*, or overall level of hypoxia in these smaller tumors (Fig. 6.11G) was too low to induce sensitivity to **1**. The latter hypothesis is supported by comparable HIF-1a levels in non-necrotic regions of GBM39 tumors from a group treated according to *Schedule C* (Fig. 6.11A) and by tendency of smaller tumors to be less hypoxic (43). Overall, effects of **1** on apoptosis and proliferation are consistent with expected results of inhibition of hypoxic response and reduced microvessel density.

Effects on gene expression. Compound **1** reduced mRNA expression of a panel of genes involved in angiogenesis and metastasis. Many of the affected genes carry important functions in tumor adaptation to hypoxia; for example, Platelet-derived growth factor subunit B (*PDGFB*) and Angiopoietin-1 are involved in blood vessel maturation (4), whereas Lysyl Oxidase (*LOX*) or *RHOC* were involved in metastasis (44, 45). We also observed a slight elevation (1.4-fold) in both mRNA expression and serum concentration of *VEGF*, despite a visible downregulation in tissue culture (17). Reduction in microvessel density typically leads to decreased oxygen pressure and increased expression of proangiogenic factors, including *VEGF* (4, 39). However, it is not obvious whether elevation would be higher had it not been for treatment with **1**. Interestingly, elevated expression of *VEGF* did not prevent **1** from exerting antiangiogenic effect, suggesting that its mechanism of action could be *VEGF*-independent.

Conclusions

In summary, this study demonstrates that Py-Im polyamide **1** interferes with several aspects of hypoxic response *in vivo*. Investigation of its *in vivo* mechanism of action suggests that **1** inhibits many endpoints of the hypoxic response in tumors: prometastatic and proangiogenic gene expression, tumor cell apoptosis in HIF-1 α positive areas, decrease in nuclear density and proliferative index and microvessel density. This compound could potentially be useful in treatment of HIF-1 related disease as it distributes to tissues and has favorable pharmacokinetics, antitumor, and antiangiogenic activity in two different xenografts.

Materials and methods

Pharmacokinetic and toxicity experiments. Animal experiments were carried out according to approved Institutional Animal Care and Use Committee protocols at the California Institute of Technology (Pasadena, CA). PK studies were done as previously described (28). In short, 6.8 mg/kg of **1** was administered s.c. in C57BL6 mice (CRL) and blood was collected retroorbitally (RO) at 1.5h, 4h and 48h. Serum was cleared by centrifugation (850g, 5 min), **1** extracted with 50% methanol and concentration analyzed by HPLC. Serum for analysis of toxicity markers (IDEXX) was obtained by RO collection and centrifugation (2000g, 15 min) in Serum Separator Tubes (BD Biosciences). The radioquantitation of **2** was performed as described elsewhere (46).

Table 5.2 Primers used in RT-qPCR experiments

Transcript	Forward (5'-3')	Reverse (5'-3')
<i>ANGPT1</i>	AGCGCCGAAGTCCAGAAAAC	TACTCTCACGACAGTTGCCAT
<i>ANGPT2</i>	AACTTTCGGAAGAGCATGGAC	CGAGTCATCGTATTTCGAGCGG
<i>bFGF</i>	AGAAGAGCGACCCTCACATCA	CGGTAGCACACACTCCTTTG
<i>EGF</i>	TGGATGTGCTTGATAAGCGG	ACCATGTCCTTTCCAGTGTGT
<i>ET2</i>	CGTCCTCATCTCATGCCAAG	AGGCCGTAAGGAGCTGTCT
<i>FLT1</i>	CAGCAACATGGGAAACAGAAT	TAGAGTCAGCCACAACCAAGG
<i>GAPDH</i>	AGAAGGCTGGGGCTCATTG	AGGGGCCATCCACAGTCTTC
<i>HOXB9</i>	CCATTTCTGGGACGCTTAGCA	TGTAAGGGTGGTAGACGGACG
<i>LOX</i>	AAGGTTTCTCAGCAAAGTACA	GACATCTGCCCTGTATGCTGT
<i>MMP14</i>	GGCTACAGCAATATGGCTACC	GATGGCCGCTGAGAGTGAC
<i>MMP2</i>	TACAGGATCATTGGCTACACACC	GGTCACATCGCTCCAGACT
<i>mTie2</i>	CAGCTTGCTCCTTTATGGAGTAG	ATCAGACACAAGAGGTAGGGAAT
<i>NEDD9</i>	ATGGCAAGGGCCTTATATGACA	TTCTGCTCTATGACGGTCAGG
<i>NRLGN1</i>	GGTGCCCCATTGACTCTCTG	GTGGGTCCACATCATCCAATTTT
<i>NRP2</i>	GCTGGCTATATCACCTCTCCC	TCTCGATTTCAAAGTGAGGGTTG
<i>PDGFB</i>	CTCGATCCGCTCCTTTGATGA	CGTTGGTGCGGTCTATGAG
<i>PGF</i>	GAACGGCTCGTCAGAGGTG	ACAGTGCAGATTCTCATCGCC
<i>RHOC</i>	GGAGGTCTACGTCCCTACTGT	CGCAGTCGATCATAGTCTTCC
<i>VEGF</i>	AGGGCAGAATCATCACGAAG	GGTACTCCTGGAAGATGTCC

Quantitative Real Time-Reverse Transcription-PCR assay. Primers (Table 2)

were designed using Harvard Primer bank (47). The total mRNA in tumors was extracted, analyzed and processed as in our previous studies (29).

Cell culture experiments

General Maintenance. Cell lines were characterized by StemElite ID system (Laragen). Temozolomide (TMZ) resistance of U251 cells has been assessed by Sulforhodamine B Assay (SRB) by plating 2k U251 cells per well in 96-well plates, allowing cells to attach for 24 h and then dosing TMZ up to 2 mM for 72 h. Obtained values of IC50 (sigmoidal fit) indicated TMZ resistance ($IC_{50} = 252 \pm 60 \mu M$, 95% CI, n=6). U251 cells were maintained as adherent culture in RPMI-1640 medium (Gibco) supplemented with 10% FBS. They were sub-cultured at a ratio of 1:4-1:10 every 3 days. B) GBM39 cells were cultured as suspension culture in neurosphere growth medium, defined as F12/DMEM medium (Gibco) supplemented with b27 (diluted to 1x from a 50x solution, Gibco), EGF (20 ng/ml final, Life Technologies), bFGF (20ng/ml final, Life Technologies), heparin (50 $\mu g/ml$ final, Sigma Aldrich) and Glutamax (diluted to 1x from a 100x solution, Life Technologies). The EGF and bFGF growth factors were replenished every two days at concentrations listed above in presence of heparin. GBM39 cells were maintained in cell culture for up to 25 passages. After which GBM39 cell culture was re-established from a subcutaneous xenograft ($\sim 500 \text{ mm}^3$, male NSG, see also the xenograft methods section). The tumor was disintegrated mechanically, digested enzymatically (10% accutase in F12-K for 3 hours), and cells further disaggregated by pipetting. The cells were then cultured as described above. Human umbilical vein endothelial cells (HUVEC) were cultured in

200 PRF medium (Gibco) supplemented with Low Serum Growth Supplement (LSGS, Invitrogen). Media was exchanged every 48 h and passaged weekly. **Tube formation assay.** HUVEC cells were plated at 2×10^5 cells per 75cm flask. After 36 hours, Py-Im polyamide **1** was added at a 5 μM final concentration, and cells incubated for 72 hours. Twelve-well plates were coated with 100 μl Geltrex (reduced growth factor basement membrane, Invitrogen) per well and allowed to solidify at 37°C for 60 min. Cells were trypsinized and taken up in 200 PRF medium at $2 \times 10^5 \text{ mL}^{-1}$, and plated in the 12-well plates at 400 μL per well. After 6-12 hours the wells were imaged on an inverted microscope by selecting 4 random fields of view.

Xenograft establishment and measurement

Male NOD-SCID-Gamma (NSG, NOD.Cg-Prkdcscid Il2rgtm1Wjl/SzJ) mice were purchased from Jackson Laboratories (JAX) and kept under defined flora pathogen-free conditions at the Association for Assessment of Laboratory Animal Care–approved Animal Facility at California Institute of Technology. U251 or GBM39 cells were implanted subcutaneously (s.c.) into left flanks of NSG mice as disaggregated cell suspensions of 2.5×10^6 (U251) in RPMI-1640 medium or 7.5×10^5 (GBM39) in 50% matrigel/neurosphere growth medium, using a g26 needle. Xenograft-bearing animals were treated once tumors had reached a minimum volume of 50 mm^3 as assessed by a caliper measurement ($\sim 60 \text{ mm}^3$ for U251 (Schedule A), and $\sim 80 \text{ mm}^3$ (Schedule B); $\sim 100 \text{ mm}^3$ for GBM39 xenografts). Each vehicle-treated control xenograft was paired with a xenograft of the same initial volume to be treated with **1**. Treatment was conducted by s.c. injection into the interscapular area (20% DMSO/PBS vehicle, or a stock solution of **1** at a concentration of 670 μM). Injected volumes were adjusted for animal weight, as specified *Schedule A-C*).

Animal weights were monitored at least once a week (see Supplementary Figure 1).

Compound was administered s.c. interscapularly in 20% DMSO/PBS. Mice were euthanized if 15% weight loss, or more was observed.

Immunohistochemistry and histologic analysis

Immunohistochemistry and tumor sectioning was conducted at the Tissue Processing Core Laboratory (TPCL) at UCLA using protocols established at TPCL. Tumors were harvested 72 h following the last administration of **1** or vehicle, embedded in paraffin and sectioned to 5 μ m thickness. Tumor microvessels were visualized using anti-mouse CD31 staining using SC-1506 antibody (SCBT) and apoptosis was assayed for using anti-human Cleaved-Caspase-3 (CC3) antibody (9664, CellSignal) and HIF-1 α using CME 349 A (Biocare Medical). At least two tissue sections per slide were used for each experiment. Slides were scanned using an Aperio ScanScope AT (Aperio, Vista, CA) at a constant illumination and exposure. Images were then processed using ImageScope.

Perinecrotic area was defined as a field of view at 20x magnification that contained 50% necrosis and 50% adjacent, non-necrotic area, with edge of necrosis in the middle of the screen. Number of histologic measurements for each tissue section were chosen to limit variability of the final average value to <10%, per tumor, or until all available data in the section was counted. Measurements were averaged for each tumor, after which statistical analysis was performed for the obtained averages. All immunostaining quantifications were done at 20x magnification, unless otherwise noted.

At least 6 (CC3) or 9 (CD31) fields of view per tumor chosen randomly prior to analysis, at either 20x (CC3 staining, CD31 staining for U251, GBM39, *Schedules A and B*) or 40x

magnification (CD31 staining for GBM39, *Schedule C*, due to higher CD31 positive vessel counts). For analysis of frequency of apoptotic blood vessels (CC3/CD31 double staining), we counted enough high power fields (20x) containing CD31 positive vessels, to assess at least 600 microvessels per condition. Perinecrotic MVD was measured by first delineating nuclei on the edge of necrosis, and then offsetting the obtained path by an equivalent of 50 μm -350 μm , by an automatic algorithm in Adobe Illustrator CS5. The MVD was then counted manually for each 50 μm thick zone. Area of each zone was measured by an automatic integration of images and converted to mm^2 , in order to obtain MVD values. At least 40 measurements per tumor were obtained, with a total of 854 measurements for a group treated with **1** and 586 for a group treated with vehicle. Measurements of the nearest blood vessel-necrosis distance were done manually using ImageScope software at 40x magnification. For GBM39 tumors, 329 measurements (n=6 per condition) were performed and 474 (n=10 per condition) measurements were done for U251 tumors. Fields of view measured per tumor section varied depending on the amount of available necrotic regions with a well-defined, and thus quantifiable, border. Number of measured values per tumor section ranged between 16 and 53. Both HIF-1 and CC3 positive pixel counts were done by choosing at least 8 random fields of view at 20x magnification. Perinecrotic areas included at least n=8 measurements per tumor section and non-necrotic areas used at least n=10 per tumor section, and were higher whenever the amount of necrotic regions in the section allowed for it. Ki-67 measurements were done using Immunoratio software (48) at 20x magnification, with n=24 per tumor section. Nuclear density (and by proxy – necrosis) was assessed by automatic nuclei counting using

Image-based Tool for Counting Nuclei (ITCN), 16 fields of view were analyzed per tumor section.

Pharmacokinetics

Determination of serum concentration of **1** was performed as described previously (28). In short, **1** was injected subcutaneously into interscapular area at 6.8 mg/kg, which corresponds to 7.5 $\mu\text{mol/kg}$ body weight. Blood was collected retroorbitally either at 1.5h, 4h or 48h after administration and allowed to clot for 30 minutes and centrifuged at 850 x g for 5 minutes. Serum was then mixed with two volume equivalents of methanol, vortexed and the resultant suspension centrifuged (16000 x g, 5 min). Supernatant solutions were diluted 1:1 with the HPLC loading buffer (water:acetonitrile, 80:20, acidified with 0.08 trifluoroacetic acid) and injected onto an analytical HPLC (Beckmann). Boc-Py-OMe was used as the internal standard.

Polyamide uptake and distribution *in vivo*

C-14 Radioquantitation. Quantification was performed in line with our previously reported metho. Briefly, tumor-bearing animals were injected with 6.8 mg/kg C-14 radiolabeled Py-Im polyamide **2**. After 24 hours, tissues with typical weights not exceeding 300 mg per sample were dissolved in 1 mL of the tissue solubilizing mixture SOLVABLE (Perkin-Elmer) overnight. Solutions were subsequently decolorized with 400 μl H₂O₂ (30 % w/w aqueous solution) per sample, for 1-2 hours at room temperature, then for 1 hour in 55-65 °C. HIONICFLUOR was added at 10 mL per sample and vials vortexed vigorously. Radioactivity associated with tumors, livers, kidneys and lungs was quantitated by liquid

scintillation counting on a Beckman Coulter LS6500 Multi-Purpose Scintillation Counter and quench-adjusted, as reported elsewhere (46). **Nuclear localization.** Mice were administered Py-Im polyamide **3** in three injections, every second day at 8.2 mg/kg (5 μ moles/kg). Twenty four hours post last injection tissues were harvested, fixed in formaldehyde for 24-48 hours and subsequently cryoprotected, first in 15% and then 30% aqueous sucrose (24 hours for each step). Tissue blocks were embedded in Tissue-Tek O.C.T. cryoembedding medium and sectioned at 5-10 μ m of thickness. Slides were imaged on a confocal microscope capable of fluorescence detection (Zeiss LSM 510) under 63x oil immersion objective.

***In vivo* gene expression analysis, and RNA extraction**

The procedure for extraction and analysis was described elsewhere (29). In short, NSG mice bearing U251 xenografts were asphyxiated, tumors extracted and snap-frozen in LN2. They were subsequently homogenized using Tissue Tearor (BioSpec) and extracted using Trizol Plus kit, according to manufacturer's instructions. Reverse-Transcription was performed using First-Strand Transcriptor kit (Roche), using 1 μ g of total RNA per reaction. RT-qPCR analysis was performed on ABI 7300 thermal cycler, using primers designed by Harvard PrimerBank and SYBR Green RT-PCR master mix (Life Technologies) and *GAPDH* as a house keeping gene as it levels were shown to be unaffected by hypoxia in U251 cells (49). For analysis of serum levels of VEGF proteins, NSG mice were dosed according to *Schedule A*, blood collected retroorbitally and serum

cleared by centrifugation (850g, 5 min). Subsequently, the VEGF protein level was measured using human-VEGF ELISA kit (R&D Biosciences).

Statistical Analysis

Each sample was analyzed using a two-tailed, student's t-test, assuming normality and unequal variance. P-value of 0.05 or less was considered statistically significant. All error bars on mean values shown are 95% confidence intervals (CI95%) and all error bars on medians, represent 25th-75th percentiles.

Acknowledgements

U251 cell line was a gift of Dr. Giovanni Mellilo (NCI). GBM39 cells were a gift of Dr. David Akhavan (UCLA), originally obtained from Prof. David James (UCSF). The authors thank Caltech OLAR for technical assistance with animal experiments and TPCL (UCLA) for assisting with IHC. The authors thank Drs. Nora Rozengurt and Dinesh Rao (UCLA) for helpful suggestions, discussion and preliminary pathological evaluation of tumor sections. We thank Drs. Nicholas Nickols and Bogdan Olenyuk for helpful discussions and suggestions. This work was supported by the NIH Grant GM-51747. J.O.S. was supported by NIH GM-51747. J.A.R received postdoctoral support from the Alexander von Humboldt foundation.

References

1. Semenza GL (2014) Oxygen sensing, hypoxia-inducible factors, and disease pathophysiology. *Annu Rev Pathol* 9:47-71.
2. Siegel R, Naishadham D, & Jemal A (2013) Cancer statistics, 2013. *CA Cancer J Clin* 63(1):11-30.
3. Xia Y, Choi HK, & Lee K (2012) Recent advances in hypoxia-inducible factor (HIF)-1 inhibitors. *Eur J Med Chem* 49:24-40.
4. Loges S, Schmidt T, & Carmeliet P (2010) Mechanisms of resistance to anti-angiogenic therapy and development of third-generation anti-angiogenic drug candidates. *Genes Cancer* 1(1):12-25.
5. Wilson WR & Hay MP (2011) Targeting hypoxia in cancer therapy. *Nat Rev Cancer* 11(6):393-410.
6. Vaupel P & Mayer A (2007) Hypoxia in cancer: significance and impact on clinical outcome. *Cancer Metastasis Rev* 26(2):225-239.
7. Semenza GL, Neufeldt MK, Chi SM, & Antonarakis SE (1991) Hypoxia-inducible nuclear factors bind to an enhancer element located 3' to the human erythropoietin gene. *Proc Natl Acad Sci U S A* 88(13):5680-5684.
8. Wang GL, Jiang BH, Rue EA, & Semenza GL (1995) Hypoxia-inducible factor 1 is a basic-helix-loop-helix-PAS heterodimer regulated by cellular O₂ tension. *Proc Natl Acad Sci U S A* 92(12):5510-5514.
9. Brown JM & Wilson WR (2004) Exploiting tumour hypoxia in cancer treatment. *Nat Rev Cancer* 4(6):437-447.
10. Onnis B, Rapisarda A, & Melillo G (2009) Development of HIF-1 inhibitors for cancer therapy. *J Cell Mol Med* 13(9A):2780-2786.
11. Kung AL, *et al.* (2004) Small molecule blockade of transcriptional coactivation of the hypoxia-inducible factor pathway. *Cancer Cell* 6(1):33-43.
12. Kushal S, *et al.* (2013) Protein domain mimetics as in vivo modulators of hypoxia-inducible factor signaling. *Proc Natl Acad Sci U S A* 110(39):15602-15607.
13. Lao BB, *et al.* (2014) In vivo modulation of hypoxia-inducible signaling by topographical helix mimetics. *Proc Natl Acad Sci U S A* 111(21):7531-7536.
14. Lee K, *et al.* (2009) Acriflavine inhibits HIF-1 dimerization, tumor growth, and vascularization. *Proc Natl Acad Sci U S A* 106(42):17910-17915.
15. Kong D, *et al.* (2005) Echinomycin, a small-molecule inhibitor of hypoxia-inducible factor-1 DNA-binding activity. *Cancer Res* 65(19):9047-9055.
16. Olenyuk BZ, *et al.* (2004) Inhibition of vascular endothelial growth factor with a sequence-specific hypoxia response element antagonist. *Proc Natl Acad Sci U S A* 101(48):16768-16773.
17. Nickols NG, Jacobs CS, Farkas ME, & Dervan PB (2007) Modulating hypoxia-inducible transcription by disrupting the HIF-1-DNA interface. *ACS Chem Biol* 2(8):561-571.
18. Lee K, *et al.* (2009) Anthracycline chemotherapy inhibits HIF-1 transcriptional activity and tumor-induced mobilization of circulating angiogenic cells. *Proc Natl Acad Sci U S A* 106(7):2353-2358.
19. White S, Szewczyk JW, Turner JM, Baird EE, & Dervan PB (1998) Recognition of the four Watson-Crick base pairs in the DNA minor groove by synthetic ligands. *Nature* 391(6666):468-471.

20. Hsu CF, *et al.* (2007) Completion of a Programmable DNA-Binding Small Molecule Library. *Tetrahedron* 63(27):6146-6151.
21. Nickols NG & Dervan PB (2007) Suppression of androgen receptor-mediated gene expression by a sequence-specific DNA-binding polyamide. *Proc Natl Acad Sci U S A* 104(25):10418-10423.
22. Muzikar KA, Nickols NG, & Dervan PB (2009) Repression of DNA-binding dependent glucocorticoid receptor-mediated gene expression. *Proc Natl Acad Sci U S A* 106(39):16598-16603.
23. Raskatov JA, *et al.* (2012) Modulation of NF-kappaB-dependent gene transcription using programmable DNA minor groove binders. *Proc Natl Acad Sci U S A* 109(4):1023-1028.
24. Nickols NG, *et al.* (2013) Activity of a Py-Im polyamide targeted to the estrogen response element. *Mol Cancer Ther* 12(5):675-684.
25. Yang F, *et al.* (2013) Antitumor activity of a pyrrole-imidazole polyamide. *Proc Natl Acad Sci U S A* 110(5):1863-1868.
26. Martinez TF, *et al.* (2015) Replication stress by Py-Im polyamides induces a non-canonical ATR-dependent checkpoint response. *Nucleic Acids Res* 42(18):11546-11559.
27. Synold TW, *et al.* (2012) Single-dose pharmacokinetic and toxicity analysis of pyrrole-imidazole polyamides in mice. *Cancer Chemother Pharmacol* 70(4):617-625.
28. Raskatov JA, Hargrove AE, So AY, & Dervan PB (2012) Pharmacokinetics of Py-Im polyamides depend on architecture: cyclic versus linear. *J Am Chem Soc* 134(18):7995-7999.
29. Raskatov JA, *et al.* (2012) Gene expression changes in a tumor xenograft by a pyrrole-imidazole polyamide. *Proc Natl Acad Sci U S A* 109(40):16041-16045.
30. Raskatov JA, Szablowski JO, & Dervan PB (2014) Tumor xenograft uptake of a pyrrole-imidazole (py-im) polyamide varies as a function of cell line grafted. *J Med Chem* 57(20):8471-8476.
31. Yang F, *et al.* (2013) Animal toxicity of hairpin pyrrole-imidazole polyamides varies with the turn unit. *J Med Chem* 56(18):7449-7457.
32. Jacobs VL, Valdes PA, Hickey WF, & De Leo JA (2011) Current review of in vivo GBM rodent models: emphasis on the CNS-1 tumour model. *ASN Neuro* 3(3):e00063.
33. Hu YL, *et al.* (2012) Hypoxia-induced autophagy promotes tumor cell survival and adaptation to antiangiogenic treatment in glioblastoma. *Cancer Res* 72(7):1773-1783.
34. Akhavan D, *et al.* (2013) De-repression of PDGFRbeta transcription promotes acquired resistance to EGFR tyrosine kinase inhibitors in glioblastoma patients. *Cancer Discov* 3(5):534-547.
35. Sarkaria JN, *et al.* (2006) Use of an orthotopic xenograft model for assessing the effect of epidermal growth factor receptor amplification on glioblastoma radiation response. *Clin Cancer Res* 12(7 Pt 1):2264-2271.
36. Tentler JJ, *et al.* (2012) Patient-derived tumour xenografts as models for oncology drug development. *Nature reviews. Clin Oncol* 9(6):338-350.
37. Blagosklonny MV (2004) Antiangiogenic therapy and tumor progression. *Cancer Cell* 5(1):13-17.
38. Tang CM & Yu J (2013) Hypoxia-inducible factor-1 as a therapeutic target in cancer. *J Gastroenterol Hepatol* 28(3):401-405.
39. Rapisarda A, *et al.* (2009) Increased antitumor activity of bevacizumab in combination with hypoxia inducible factor-1 inhibition. *Mol Cancer Ther* 8(7):1867-1877.

40. Thomlinson RH & Gray LH (1955) The histological structure of some human lung cancers and the possible implications for radiotherapy. *Br J Cancer* 9(4):539-549.
41. Ryan HE, Lo J, & Johnson RS (1998) HIF-1 alpha is required for solid tumor formation and embryonic vascularization. *EMBO J* 17(11):3005-3015.
42. Presta LG, *et al.* (1997) Humanization of an anti-vascular endothelial growth factor monoclonal antibody for the therapy of solid tumors and other disorders. *Cancer Res* 57(20):4593-4599.
43. Lyng H, Skretting A, & Rofstad EK (1992) Blood flow in six human melanoma xenograft lines with different growth characteristics. *Cancer Res* 52(3):584-592.
44. Erler JT, *et al.* (2006) Lysyl oxidase is essential for hypoxia-induced metastasis. *Nature* 440(7088):1222-1226.
45. Sethi N & Kang Y (2011) Unravelling the complexity of metastasis - molecular understanding and targeted therapies. *Nat Rev Cancer* 11(10):735-748.
46. Raskatov JA, Puckett JW, & Dervan PB (2014) A C-14 labeled Py-Im polyamide localizes to a subcutaneous prostate cancer tumor. *Bioorg Med Chem* 22(16):4371– 4375
47. Spandidos A, Wang X, Wang H, & Seed B (2010) PrimerBank: a resource of human and mouse PCR primer pairs for gene expression detection and quantification. *Nucleic Acids Res* 38(Database issue):D792-799.
48. Tuominen VJ, Ruotoistenmaki S, Viitanen A, Jumppanen M, & Isola J (2010) ImmunoRatio: a publicly available web application for quantitative image analysis of estrogen receptor (ER), progesterone receptor (PR), and Ki-67. *Breast Cancer Res* 12(4):R56.
49. Said HM, *et al.* (2007) GAPDH is not regulated in human glioblastoma under hypoxic conditions. *BMC Mol Biol* 8:55.